IN VITRO AND *IN VIVO* CHARACTERISATION OF ISOLATES OF *CRYPTOCOCCUS NEOFORMANS* CAUSING MENINGITIS IN HIV INFECTED AND UNINFECTED PATIENTS IN VIETNAM

Lam Tuan Thanh [1], Dena Toffaletti[2], Jennifer Tenor[2], Charles Giamberardino[2], Gregory D. Sempowski[3], Yohannes Asfaw[4], Hai Trieu Phan[1], Anh Van Duong[1], Trinh Mai Nguyen[1], Lan Phu Huong Nguyen [5],Chau Thi Hong Tran [1], Philip M. Ashton[1], Justin Beardsley[1],Chau Van Vinh Nguyen [6], Guy E. Thwaites[1], Stephen Baker[1], John R. Perfect[2], Jeremy N. Day[1,5]

[1]Oxford University Clinical Research Unit, Hospital for Tropical Diseases, Ho Chi Minh City, Vietnam

[2]Division of Infectious Diseases, Department of Medicine and Department of Molecular Genetics and Microbiology, Duke University, North Carolina, USA

[3]Duke Human Vaccine Institute and Regional Biocontainment Laboratory, Duke University, North Carolina, USA

[4]Division of Laboratory Animal Resources, Duke University, North Carolina, USA

[5]Nuffield Department of Clinical Medicine, Centre for Tropical Medicine and Global Health, University of Oxford, Oxford, UK

[6]Hospital for Tropical Diseases, Ho Chi Minh City, Vietnam

Corresponding author: Jeremy N Day: jday@oucru.org

Running title: Characterizing *Cryptococcus neoformans* from HIV uninfected patients

Keywords

Cryptococcal meningitis, *Cryptococcus neoformans,* MLST, immunocompetent, HIV-uninfected, HIV, A/J mice, ST5, phenotype

Abstract

Most cryptococcal meningitis occurs in immunocompromised individuals and is caused by *Cryptococcus neoformans* var. *grubii.* We previously reported cryptococcal meningitis in Vietnam arising atypically in HIV-uninfected, apparently immunocompetent patients, caused by a single amplified fragment length polymorphism (AFLP) cluster of *C. neoformans* (termed VNI-γ). This variant was less common in HIV-infected individuals. It is unclear why this lineage is associated with HIV-uninfected, apparently immunocompetent patients. To better delineate the phenotypic characteristics of *C. neoformans* VNI-γ in comparison with other *C. neoformans* lineages we selected 30 representative isolates and compared their genotype-specific *in vitro* pathogenic potential and *in vivo* virulence, and ability to induce inflammatory response in the A/J mouse model. All isolates were genotyped using multi-locus sequence typing. All previously AFLP-defined VNI-γ isolates were identified as sequence type (ST) 5. Compared with non-ST5 strains, ST5 isolates had significantly increased variability in cell and capsule size (p<0.001). ST5 and non-ST5 strains exhibited similar characteristics in relation to previously defined virulence factors including melanization, growth at 37°C, and growth in cerebrospinal fluid. However, A/J mice infected with ST5 isolates had significantly longer survival and lower fungal burdens at day 7 and death compared with non-ST5 isolates. ST5 isolates induced significantly greater initial

inflammatory responses than non-ST5 strains, measured by TNF-α concentrations (p<0.001). Despite being generally less virulent in the mouse model, we hypothesize that the significant within strain variation seen in ST5 isolates in the tested phenotypes may represent an evolutionary advantage enabling adaptation to novel niches including apparently immunocompetent human hosts.

Introduction

Cryptococcal meningitis (CM) is a life-threatening fungal infection occurring in immunocompromised individuals including those with HIV infection, malignancy, organ failure, autoimmune disease and people receiving immunomodulatory therapy (1–3). Recent estimates indicate a global annual CM incidence in HIV infected patients of 223,100 cases, resulting in 181,100 deaths (4). The burden of CM is highest in sub-Saharan Africa and South/Southeast Asia where there are substantially more people living with HIV/AIDS (4). *Cryptococcus neoformans* and *Cryptococcus gattii* are the two main etiologic agents for CM globally. *C. gattii* most often causes infection in apparently immunocompetent patients while *C. neoformans* is primarily responsible for disease in immunocompromised patients (5). In tropical and subtropical regions, *C. gattii* CM is relatively uncommon in HIV-infected patients, usually accounting for only 1-2% of cryptococcosis in HIV-infected individuals, though higher rates have been reported from Botswana and Malawi (up to 30% of all CM cases) (6, 7). Where CM due to *C. neoformans* var. *grubii* occurs in HIV-uninfected individuals, reports often describe patients with an increased disease susceptibility due to other underlying immunosuppressive conditions

(8, 9). However, reports of non-HIV CM from Australasia and the USA indicated no clear underlying immune deficit in approximately 20% of cases (10–12). In Vietnam, disease in HIV-uninfected patients accounts for approximately 10% of all CM cases admitted to our referral hospital in Ho Chi Minh City (HCMC) (13). We have previously reported that the majority of HIV-uninfected patients had no identified cause of immunosuppression, and that >80% of HIV-uninfected CM patients were infected by yeasts belonging to a single Amplified Fragment Length Polymorphism (AFLP)-defined cluster of *C. neoformans* var. *grubii*, which we had named VNIγ(14). Further phylogenetic characterization by multi-locus sequence typing (MLST) confirmed that the isolates from apparently immunocompetent patients were significantly associated with the monophyletic sequence type 5 lineage (ST5), and that all isolates form the VNIγ cluster were ST5 (15). Our clinical observation has been replicated in China where over 70% of CM cases from apparently immunocompetent individuals were infected with *C. neoformans* (16, 17). The yeasts isolated from immunocompetent patients in China were closely related to each other and were all attributed to the ST5 genotype (18, 19). Similarly, this sequence type accounted for more than 80% of non-HIV-associated cases of CM in South Korea, although some patients from this group had other underlying, potentially immunosuppressive conditions (20). The association between a particular ST/genotype and host immune phenotype could be explained by a lineage-specific increase in pathogenic potential or microbial fitness, a currently unidentified host immune deficit, or a combination of these factors.

Here, in order to explore the hypothesis that ST5 strains have increased pathogenic potential, we compared their virulence phenotypes with non-ST5 strains in a range of *in vitro* experiments. Additionally, we used a mouse model of cryptococcosis to compare the relative *in*

vivo virulence of, and immune responses to, Vietnamese VNIγ/ST5 and non-VNIγ/ST5 clinical isolates.

Material and methods

C. neoformans isolates and culture conditions

We used clinical isolates obtained at the point of diagnosis, prior to antifungal therapy, from the cerebrospinal fluid (CSF) of patients enrolled in a prospective descriptive study of HIV-uninfected patients with central nervous system (CNS) infections, and a randomized controlled trial of antifungal therapy in HIV-infected patients (13, 21). All studies were approved by the Institutional Review Board of the Hospital for Tropical Diseases, Ho Chi Minh City, Vietnam and the Oxford Tropical Ethics Committee or Liverpool School of Tropical Medicine (UK). Bulk isolate from each patient was kept at -80°C using Microbank beads (Pro-Lab Diagnostics, UK). Isolates were single-colony-purified for all subsequent experiments. We randomly selected 15 isolates from our HIV uninfected cohort of patients. This resulted in 13 apparently immunocompetent patients (all infected with AFLP VNIγ strains) and 2 patients with underlying disease, infected with VNIδ strains (15 in total). We then randomly selected 2 HIV patients with VNIγ infection and 13 HIV patients with VNIδ infections, to deliver 30 isolates in total, 15 of each AFLP cluster. Mating type, AFLP fingerprints and 7-digits consensus MLST profiles (CAP59, GPD1, IGS1, LAC1, PLB1, SOD1, URA5) for all isolates were previously determined (15). *C. neoformans* yeasts were propagated using Yeast Peptone Dextrose (YPD) broth and incubated overnight at 30°C with agitation. Cells were harvested and washed 3 times in phosphate-buffered saline (PBS).

Inoculum was quantified using a Cellometer X2 cell-counter (Nexelom Biosciences, USA). Isolates and clinical information from corresponding patients were summarized in Table 1.

Growth at high temperature, in *ex vivo* human CSF and melanin production

Growth at high temperature and in *ex vivo* human CSF were tested as previously described (22) with modifications for quantitative assessment. To assess fungal growth at different temperatures, the inoculum was adjusted to 10^8 cells/ml, serially diluted and spot-inoculated in duplicate on YPD agar in 5µl aliquots and incubated at 30°C or 37°C for 48 hours. After 48 hours, colony forming units (CFU) were counted and recorded in CFU/ml. For the *ex vivo* CSF growth assay, baseline pre-antifungal treatment CSF supernatant from random de-identified HIV-infected patients enrolled into an antifungal therapy trial was pooled, filtered, and stored at -80°C until use. 10µl of 10^8 cells/ml yeast suspension was inoculated into 90µl of pooled CSF and incubated at 37°C with 5%CO_2. Inoculated CSF was serially diluted and spotted on YPD agar at days 1 and 3 post-inoculation. All experiments were repeated in triplicate. The H99-derived mutant *Δena1*, which lacks a cation-ATPase-transporter resulting in decreased viability in human CSF and macrophages, was used as a negative control for the *ex vivo* CSF assay (23). H99 was included as a reference in all experiments. Data were standardized by expressing the results as a ratio of the CFU/ml of the test isolate to the CFU/ml of H99. Melanin production was assessed by plating 5µl of 10^6cells/mL cell suspension on L-DOPA agar containing 1g/L L-asparagine , 1g/L glucose, 3g/L KH_2PO_4, 250mg/L $MgSO_4.7H_2O$, 1mg/L Thiamine HCl, 5µg/L Biotin, 100mg/L L-DOPA, 20g/L Bacto Agar (24, 25). Plates were incubated in the dark at 30°C or 37°C for 3 days. Differences in colony melanization were compared visually with reference to

126 H99 and an H99-derived mutant with diminished melaninization in L-DOPA agar from the
127 Perfect lab.

128 **Extracellular urease and phospholipase activity**

129 Extra-cellular urease production was semi-quantified using Christensen's agar. 10µl of 10^8
130 cells/ml yeast suspension was spotted on Christensen's agar and incubated at room
131 temperature. The time to complete plate colouration was determined using a GoPro Hero 6
132 camera (Gopro, USA) using the time-lapse setting set with a 1 minute interval. *C. neoformans*
133 H99 was used as a positive control and *Candida albicans* as a negative control. Extracellular
134 phospholipase activity was screened on egg yolk medium as previously described, with minor
135 modifications (26). The egg yolk medium contained Sabouraud agar with 1M sodium chloride,
136 0.005M calcium chloride and 8% sterile egg yolk enrichment (Merck, USA). A 5 µl aliquot of *C.*
137 *neoformans* yeast suspension (10^8 cells/ml) was spotted on egg yolk agar and incubated at 30°C
138 for 72 hours. The diameters of the precipitation zone (D) formed around the colonies and of the
139 respective colonies (d) were recorded after 72 hours incubation. The D/d ratio for each isolate
140 was calculated. H99 was included for reference in each experimental batch. The final result for
141 each isolate was expressed as the ratio between the test isolate's D/d ratio and that of H99. All
142 isolates were tested in triplicate for each phenotype.

143

144 ***In vitro* capsule and cell size measurement**

145 To measure *in vitro* cryptococcal capsule thickness, all isolates were streaked onto capsule-
146 inducing agar containing powdered Dulbecco Modified Eagle Medium (DMEM) [supplemented

147 with 4.5g/L glucose, L-glutamine, sodium pyruvate], $NaHCO_3$ 250mM, NaMOPS 1M, Neomycin
148 200mg/ml, Cefotaxime 100 mg/ml (27). Plates were incubated at 37°C in 5% CO_2 until single
149 colonies were visible. Unless otherwise specified, all reagents were purchased from Sigma-
150 Aldrich. India ink smears from a single yeast colony were prepared on a glass slide and
151 visualized at 100X magnification using a CX41 microscope (Olympus, Japan). Images of single
152 microscopic yeast cells were captured using a DP71 Camera system with DP Controller software
153 (Olympus, Japan) and processed using ImageJ (rsb.info.nih.gov/ij/). Capsular thickness was
154 calculated by subtracting yeast cell body diameter (D_{CD}, no capsule) from whole cell diameter
155 (D_{WC}, including capsule). At least 30 individual microscopic yeast cells were assessed for each
156 isolate.

157 **Mouse inhalation infection model of cryptococcosis**

158 All mouse infection experiments were conducted as previously described according to Duke
159 University's Institutional Animal Care and Use Committee guidelines and approvals(28).
160 Six-week old female A/J mice were sedated with isoflurane and inoculated intranasally with the
161 selected *C. neoformans* var. *grubii* isolate by dropping 25µl of yeast suspension containing
162 $5x10^4$ cells into the nares. Eight isolates were randomly selected from the 30 for murine
163 experiments. The isolates were five ST5 (BK147 and BK44 from HIV infected patients and
164 BMD700, BMD1338 and BMD1646 from HIV uninfected patients) and three non-ST5 strains
165 (BMD1415 (ST4) and BMD1367 (ST306) from HIV uninfected patients and BK80 (ST4) from an
166 HIV infected patient). Animals were monitored daily and euthanized by CO_2 inhalation at
167 indicated time points (fungal burden and *in vivo* responses) or until weight loss ≥ 15% body
168 weight was observed (virulence assay).

169 **Determining *in vivo* fungal burden**

170 Five mice were infected with each isolate in two independent experiments for assessment of
171 fungal burden at 7 or 14 days post-infection. All animals in each experiment set were
172 euthanized by CO_2 inhalation either on day 7 or day 14 post-infection. Fungal burden at each
173 time point was assessed by excising the left superior lobe of the lung and brain and
174 homogenizing the tissue by bead beating. Tissue homogenate was serially diluted and plated
175 onto YPD agar supplemented with 100mg/ml ampicillin. The plates were incubated at 30°C for
176 48 hours and the number of *C. neoformans* colony forming units (CFU) recorded. Fungal
177 burdens were expressed as CFU per gram of tissue (CFU/g). At each time point, additional lung
178 lobes were also collected for determining *in vivo* histopathology and cytokine response, as
179 described below. In addition, fungal burdens were separately determined at the point of death
180 in animals from the survival assays described below.

181 **Determining *in vivo* histopathology**

182 At specific time points (7 or 14 days post-infection, as described above), the right superior lung
183 lobe from each mouse was excised and immersed in 10% formalin (replaced with 70% ethanol
184 after 24 hours) for fixation. Fixed, uninflated lung specimens were stored at 4°C until further
185 processing. After paraffin embedding, sliced sections were stained using the periodic acid-Schiff
186 (PAS) or mucicarmine stains. Histopathological examination was performed by an independent
187 pathologist blinded to infecting strain. Tissue damage was scored from 0 (no changes) to 10
188 (severe changes), corresponding to the severity of pathology in 4 different categories: necrosis,

189 hemorrhage, edema and inflammation, as per the Duke Veterinary Diagnostic Laboratory
190 (Division of Laboratory Animal Resources).

191 **Determining *in vivo* cytokine response**

192 To assess the severity of the inflammatory responses at specific time points (day 7 and day 14
193 post-infection), the middle lobe from the right lung of each infected mouse was excised and
194 homogenized by bead beating in 1ml sterile PBS/Protease inhibitor. 500µl of lung homogenate
195 was used for cytokine profiling. Cytokines representing T-helper type 1 (Th1) (IL-12p70, TNF-α,
196 IFN-γ), T-helper type 17 (IL-17) and T-helper type 2 (Th2) (IL-4, IL-5, IL-10) responses were
197 measured using a customized Bio-Plex Pro™ Mouse Cytokine Th1/Th2 Assay kit (Biorad, USA)
198 with the BioPlex 200 platform according to the manufacturer's guidelines. Data were retrieved
199 using BioPlex Manager Software. The upper and lower limits of quantification (ULOQ and LLOQ)
200 were based on a standard curve. All values falling below the LLOQ were replaced with the
201 midpoint between zero and the LLOQ. Data were standardized by lung weight and presented as
202 picogram of cytokines per gram lung tissue (pg/g).

203 ***In vivo* virulence assay**

204 The virulence assay was conducted independently from the day 7/day 14 experiment. Each of
205 the 8 selected isolates was inoculated intranasally into 10 A/J mice. Mice were monitored daily
206 until death, or loss of more than 15% body weight (impending death), at which point they were
207 euthanized by CO_2 inhalation, necropsied and had fungal burden in lung and brain determined.

208 **Statistical analysis**

209 GraphPad Prism version 5.04 for Windows (GraphPad Software, San Diego California USA;
210 www.graphpad.com) was used for data visualization and statistical analyses of fungal loads,
211 cytokine profiling, capsular/cell size, and survival proportions. The Mann-Whitney U-test was
212 used for comparing fungal load and cytokine concentrations. Kaplan-Meier survival curves and
213 the log-rank test were used for survival analysis. Capsule/cell size was compared using Welch's
214 t-test. The Fligner-Killeen test of variance homogeneity for analyzing variation in capsule/cell
215 size and Fisher's exact test were performed using R software, version 3.2.4 (http://www.r-
216 project.org). One way ANOVA with post hoc multiple comparison tests (Dunnett or Bonferroni)
217 was used to compare cytokine concentrations between individual isolates.

218 **Results**

219 **ST5 *C. neoformans* isolates have increased capsule size and variability.**

220 We compared the following *in vitro* virulence phenotypes of ST5 and non-ST5 isolates: capsule
221 size, extracellular urease and phospholipase production, melanin production, growth at high
222 temperature, and in pooled human CSF. ST5 *C. neoformans* yeast cells developed significantly
223 thicker capsules during *in vitro* culture than non-ST5 isolates (Table 2). Individual ST5 *C.*
224 *neoformans* cells were also significantly larger in size than cells from the non-ST5 strains (Figure
225 1 and Table 2), and there was greater variation in both capsule size and cell diameter within ST5
226 compared with other sequence types (Figure 1, $p<0.0001$, Fligner-Killeen test). One particular
227 ST5 strain, BMD1646, was markedly larger and with thicker capsules than other isolates.
228 However, the differences in capsule thickness and cell diameter between sequence types, as

well as the variation among ST5 isolates, remained statistically significant even when this isolate was removed from the analysis (data not shown).

In contrast, there were no genotype-specific differences in the other *in vitro* phenotypes tested: growth at 30°C (p=0.10) and 37°C (p=0.23); *ex vivo* survival in CSF after 1-day (p=0.72) or 3-days exposure (p=0.77, see Supplementary Figures S1 and S2), extracellular urease activity and phospholipase activity (Supplementary Figures S3 and S4). Specific phenotyping data for the 8 isolates used for mice infection experiments are shown in Supplementary Figures S5, S6 and S7.

ST5 isolates from are less virulent than non-ST5 isolates in experimental mice infection

We tested the hypothesis that the higher prevalence of ST5 infection in apparently healthy hosts was associated with higher virulence in intranasally-inoculated A/J mice. Mice infected with ST5 strains were associated with significantly longer survival times than mice infected with non-ST5 strains (p<0.0001, Figure 2). However, there was significant variability in the effect of individual yeast strains of the same sequence type on survival (Supplementary Figure S8). Notably, two ST5 strains (BK147 and BMD1646) appeared to be substantially attenuated in comparison to other ST5 strains, with mice infected with these strains surviving up to 40 days. However, the differences in survival times between mice infected with ST5 and non-ST5 strains remained significant when these two isolates were removed from the analysis ((p=0.003, log-rank test, data not shown).

All strains successfully established lung infection and disseminated to the brain as early as day 7. Tissue-specific fungal burden data are presented in Table 3. Non-ST5 strain infections resulted in higher lung fungal burdens than ST5 infections at all time-points (for day 7, p<0.001;

for day 14 $p<0.0001$; and $p<0.0001$ at the point of sacrifice (see also Figure 3)). Again, these data were not driven by the two severely attenuated isolates (BK147 and BMD1646) as the fungal loads associated with ST5 infections remained low even when they were excluded from the analysis (data not shown). The majority of mice infected with BMD1646 (ST5) and BK147 (ST5) became sterile and therefore lung fungal burdens in these animals remained low up to day 14 (see Supplementary Figure S9 for fungal burden by individual strain). Brain fungal burdens were higher in non-ST5 strains at all time points but this was statistically significant only at the point of sacrifice (p values 0.054, 0.36 and 0.01, Mann-Whitney test, for days 7, 14 and point of sacrifice respectively).

C. neoformans isolates from HIV-uninfected patients induce higher levels of pro-inflammatory TNF-α production in the lungs of infected mice

We next measured the cytokine concentrations in lung homogenates at days 7 and 14 post-infection (Figure 4). TNF-α concentrations were significantly higher in ST5 infections than in non-ST5 strain infections ($p=0.01$; also see Table 4). Of note, the highest day 7 lung TNF-α concentrations were seen in the two ST5 strains that were most attenuated in the mouse survival model (BK147 and BMD1646), and the lowest TNF-α concentrations were measured in the most virulent ST5 isolate in the mouse model (BMD1338).

By day 14, mean TNF-α concentrations associated with the ST5 strains had declined from 3933.71 pg/g lung to 2802.36 pg/g lung ($p<0.001$). Other Th-1 cytokines including IL-12, IL-17 and IFN-γ also decreased in ST5-infected mice between days 7 and 14 ($p<0.001$, $p<0.01$ and $p=0.02$, respectively). This contrasted with non-ST5 strain infections, in which mean TNF-α levels increased from 3256.25 pg/g to 6378.76 pg/g ($p=0.02$, also see Table 4) over this time

period. However, the high concentration of TNF-α measured in non-ST5 strain infections at day 14 was driven by a single isolate - BMD1415; TNF-α concentrations in the lung in mice infected with this isolate were significantly higher than for infections with any other isolate of any lineage (p<0.001). There were no statistically significant differences in TNF-α concentrations at day 14 between lineages when this isolate was excluded from the analysis. The same BMD1415-driven pattern also occurred when comparing IFN-γ and IL-17 concentrations at day 14. The concentrations of these two cytokines in BMD1415-infected mice appeared significantly higher than in mice infected with any other isolate (p<0.001, Supplementary Figure S10). However, IL-12 concentrations fell in non-ST5-infected mice, including BMD1415, between day 7 and 14 (4 fold decrease, p<0.0001) (Figure 5).

We measured the TNF-α:IL-10 ratio as a proxy marker of the relationship between a Th-1 and a Th-2 response (29). From day 7 to day 14 post-infection, the TNF-α:IL-10 ratio decreased by a factor of 0.78 in mice infected with ST5 isolates, while those infected with non-ST5 strains exhibited an increase in the ratio of 1.25 fold. However, when BMD1415 (ST4) was excluded from the analysis the TNF-α/IL-10 ratio in non-ST5 infected mice also decreased by a factor of 0.67. By day 14 we detected elevated concentrations of IL-17 and IFN-γ in non-ST5 infected mice (5-fold and 17-fold increments, respectively (Table 4), but not in ST5 infected mice. Again, this effect was largely associated with BMD1415, since the concentrations of IL-17 and IFN-γ induced by this isolate at day 14 were significantly higher than for all others (p<0.001, see also Supplementary Figure S10).

Histopathological examination

Histological examination of infected lung tissue revealed evidence of inflammation, hemorrhage, edema and necrosis in most cases. These changes were generally greater by day 14 in comparison to day 7. There were no clear differences in histological scores between sequence types, other than strain BMB1646 (ST5) which had only mild inflammation with no necrosis or hemorrhage seen (Supplementary Figure S11). PAS staining revealed extensive perivascular infiltration of leukocytes in mice tissue associated with both infecting genotypes (BMD1338-ST5 and BMD1415-ST4, Figure 6). We did not measure genotype-specific capsule size *in vivo,* but ST5 yeasts appeared to be more extensively encapsulated than ST4 yeasts in the lung sections, especially by day 14 (Figures 6 and Figure 7).

Discussion

Most cases of cryptococcal meningitis in HIV uninfected, apparently immunocompetent, patients in Vietnam and East Asia are due to *C. neoformans* strains of multi-locus sequence type 5 (ST5) (14–16, 18, 30–32). This phenomenon could be explained either by ST5 strains being intrinsically more pathogenic, or due to unidentified lineage–specific host immune defects or exposures. It is unlikely that the high prevalence of ST5 infection observed in HIV-uninfected patients is explained by a significantly greater prevalence of the lineage in the environment since it causes only 35% of cases in HIV-infected patients within the same geographical area (14). Furthermore, data from China suggest that ST5 strains are significantly less prevalent in the environment, making up only 5% of isolates recovered in a recent study (33). We investigated the first hypothesis by comparing previously identified *in vitro* virulence-associated

313 phenotypes, along with murine *in vivo* virulence and immune responses, between lineages. All
314 isolates were derived from HIV infected or uninfected Vietnamese patients with cryptococcal
315 meningitis.

316 The comparison by MLST defined lineage is appropriate because ST5 is a coherent and distinct
317 group. It precisely aligns with the AFLP VNI-γ cluster, and whole genome sequence data reveals
318 that there are few intra-lineage genomic variations between ST5 strains (15). Furthermore, it is
319 unlikely that any phenotypic variations among ST5 isolates are primarily attributable to *subtle*
320 intra-lineage genomic variations since phenotypic and genotypic diversity are not tightly
321 coupled in *C. neoformans* var. *grubii* (34). Due to the fact that ST5 has been shown to be
322 consistently associated with the clinical phenotype of interest (infection of HIV-uninfected
323 patients), and that strains from HIV uninfected patients are dispersed throughout the VNI-γ/ST5
324 cluster, we believe the ability to infect apparently immunocompetent hosts is common to all
325 ST5 isolates. Therefore grouping strains by multi-locus sequence type for phenotypic
326 comparison was logical and likely to provide biological insights.

327 We found that isolates from all STs were able to grow in *ex vivo* human CSF and at 37°C -
328 essential characteristics for establishing human CNS infection. While these qualities would be
329 needed for disease in both HIV infected and immunocompetent patients, it might have been
330 expected that ST5 strains would grow more rapidly in these conditions. The lack of ST-specific
331 differences in these phenotypes suggests that the ability to establish disease in HIV-
332 uninfected/immunocompetent patients is not driven by simple adaptations to these conditions.

However, ST5 cells were significantly larger than non-ST5 cells, had thicker capsules *in vitro*, and had more within lineage variation in these characteristics. Capsule size and composition are known to vary during infection and under specific stress conditions (35, 36), influencing macrophage phagocytosis and modulating host immune response (36–39), and in human disease, *ex vivo* capsule size has been associated with higher intracranial pressures, slower yeast clearance and attenuated inflammation (38).While we did not formally measure yeast cell or capsule size in our *in vivo* experiments, mucicarmine staining was suggestive that capsules were indeed larger during mouse infection. It is possible that the ability of ST5 strains to cause infections in immunocompetent patients is a function of increased responsiveness to capsule-inducing conditions. Further investigation of genotype-specific characteristics of *in vitro* and *in vivo* capsular polysaccharide production, composition, and morphology, may elucidate a specific role in ST5-associated pathogenesis. Of note, cryptococcal virulence factors frequently have additional metabolic functions; the increased cell and capsule size seen in ST5 isolates may be a side effect of other processes involving capsular-biosynthesis genes (for example carbon source sensing, sugar transport and spore formation) (40, 41).

Our data indicate that phenotypic heterogeneity may be a hallmark characteristic of the ST5 lineage. Heterogeneity is a desirable trait for microbial populations under selection pressure allowing the exploitation of, and survival, in novel niches (42). Chow *et al* (2008) has previously reported that ST5 *C. neoformans* var. *grubii* possesses unique genomic features which may drive niche adaptation (43). We speculate that the phenotypic heterogeneity associated with strains from the ST5 lineage is a strategy that facilitates successful colonization of novel

354 environmental niches, and facilitates the exploitation of infrequent specific human immune
355 deficits.

356 However, paradoxically, we found no evidence that ST5 isolates have greater virulence in the
357 mouse model. There are several possible explanations. First, virulence in mice is variable
358 depending on mouse breed and may not accurately reflect the immunological heterogeneity of
359 the human population (44). Second, yeasts with different pathogenic potentials, associated
360 with their isolation from different sources (i.e. clinical versus environmental,
361 immunocompromised versus immunocompetent patients) may have the same or paradoxical
362 pathogenic potential in experimental animal models. An example is *Cryptococcus gattii* which is
363 associated with infection in immunocompetent patients and therefore is considered to be more
364 fit in the human host than *C. neoformans*. However, the hypervirulent *C. gattii* strain R265,
365 responsible for the on-going Vancouver outbreak, has similar virulence in both C57BL/6 and A/J
366 mice to the *C. neoformans* H99 strain, which was derived from a patient with Hodgkin's disease
367 on chemotherapy (45). Third, the A/J mouse breed is not immunologically intact; it may be an
368 imperfect model of infection for immunocompetent hosts (46). Rather, A/J mice may be a
369 better model of disease in immunosuppressed patients, as they are highly susceptible to
370 cryptococcal disease, and the patterns of cytokine expression in mice with disseminated
371 cryptococcosis are similar to those seen in HIV-infected patients with CM (47). Consistent with
372 this, we could not detect clinical differences in disease course or outcome between HIV patients
373 infected with ST5 versus other strains in Vietnam (15). Models that better mimic infection in
374 immunocompetent hosts are needed.

We did identify lineage specific differences in immune response in the mouse model. Previous research has suggested that a Th1 type immune response, defined by the TNF-α/IL-10 ratio, is protective, and a Th2 response is associated with poor outcomes (48, 49). We found no evidence of genotype-specific differences in TNF-α/IL-10 ratios by lineage in the murine infection model. Rather, we found higher initial (day 7) TNF-α concentrations in mice infected with ST5 isolates, suggesting this genotype elicits a more intense initial inflammatory response. Previous studies have suggested that capsule components, or cryptococcal cells themselves, have a dose-dependent ability to stimulate TNF-α production by various immune effector cells (50, 51). The more robust initial inflammatory response we observed may have been due to the ST5 capsular phenotype. Previously, it has been suggested that the ability of *C. gattii* to cause disease in apparently immunocompetent patients is because it induces a less severe inflammatory response compared with other cryptococcal species (45). The robust initial inflammatory responses seen in our murine infection experiments are not consistent with this being the mechanism underlying the ability of ST5 *C. neoformans* var. *grubii* organisms to cause disease in the immunocompetent.

In vivo controlled infection studies in mice, including ours, commonly employ the classic definition of pathogenicity as the microbe's capability to cause disease in a susceptible host, whereas virulence corresponds to the severity of the ensuing pathology (52). Using the same infective dose for all strains we failed to demonstrate that ST5 strains had greater virulence. The difference we observe in prevalence of different lineages in immunocompetent and immunosuppressed humans may actually represent specific differences in pathogenicity - the

ability of the organisms to colonize the host and establish infection. We could not assess this with our experimental system.

In summary, our cohort of ST5 *Cryptococcus* isolates displayed two notable phenotypes. First, despite their well documented ability to cause disease in HIV uninfected humans, they appeared to be less virulent in a murine model than the other sequence types, as demonstrated by reduced fungal burdens in tissue and prolonged mouse survival. Second, ST5 strains had larger capsules and cell sizes than the other genotypes, and greater variability in this phenotype throughout the lineage. These data lead us to the following conclusions. First, clinical isolates, which have by their nature already undergone selection within the human host, can possess wide variability in the expression of virulence phenotypes within a single lineage. Secondly, the use of host risk factors and immune phenotypes to derive an understanding of the factors that drive the pathogenicity of *Cryptococcus neoformans* may be more complex than anticipated. Associations may be difficult to make due to the relevance of the particular *in vitro* phenotypes, the animal models used, within strain heterogeneity, and population substructure. Moreover, there may be heterogeneity in the immune response of apparently immunocompetent patients which selects particular sub-cohorts of isolates of the same lineage. Laboratory phenotyping of larger numbers of clinical isolates is needed to define the lineage-specific differences that determine different human disease phenotypes.

Finally, it is possible that the categorization of strains into specific clades with limited genetic information such as MLST may lack precision to understand the relative fitness of specific strains in the human host. It is likely that whole genome sequencing will provide better mapping of the relationships between strains and virulence.

Conclusions

In this study, we demonstrated genotype-specific differences in *in vitro* and *in vivo* virulence phenotypes between *C. neoformans* var. *grubii* strains isolated from host with different immune status. However, there was also significant variation among strains isolated from apparently immunocompetent patients in specific *in vitro* and *in vivo* phenotypes tested. This higher rate of phenotypic variation may represent an evolutionary strategy for *C. neoformans* var. *grubii* to take advantage of novel niches and contribute to their ability to infect apparently immunocompetent hosts, despite generally being less virulent in a mammalian animal model. Furthering the understanding of the pathogenesis of cryptococcal meningitis will require investigation of large numbers of strains with associated robust clinical information, and the development of high throughput laboratory phenotypic studies that have clinical relevance in humans.

Acknowledgements

Supported by a Wellcome Trust Intermediate Fellowship awarded to JND (WT097147MA). SB is a Sir Henry Dale Fellow, jointly funded by the Wellcome Trust and the Royal Society (100087/Z/12/Z). Multiplex cytokine profiling was performed in the Immunology Unit of the Duke Regional Biocontainment Laboratory, which received partial support for construction from the US National Institutes of Health, National Institute of Allergy and Infectious Diseases (UC6-AI058607). The study was approved by the scientific committee of the Hospital for Tropical Diseases, Ho Chi Minh City, Vietnam.

438 **References**

439 1. Fang W, Chen M, Liu J, Hagen F, MS A, Al-Hatmi, Zhang P, Guo Y, Boekhout T, Deng D, Xu
440 J, Pan W, Liao W. 2016. Cryptococcal meningitis in systemic lupus erythematosus
441 patients: pooled analysis and systematic review. Emerg Microbes Infect 5:e95.

442 2. Schmalzle SA, Buchwald UK, Gilliam BL, Riedel DJ. 2016. *Cryptococcus neoformans*
443 infection in malignancy. Mycoses 59:542–552.

444 3. Williamson PR, Jarvis JN, Panackal AA, Fisher MC, Molloy SF, Loyse A, Harrison TS. 2016.
445 Cryptococcal meningitis: epidemiology, immunology, diagnosis and therapy. Nat Rev
446 Neurol 13:13–24.

447 4. Rajasingham R, Smith RM, Park BJ, Jarvis JN, Govender NP, Chiller TM, Denning DW,
448 Loyse A, Boulware DR. 2017. Global burden of disease of HIV-associated cryptococcal
449 meningitis: an updated analysis. Lancet Infect Dis 17:873–881.

450 5. Kwon-Chung KJ, Fraser JA, Doering TL, Wang ZA, Janbon G, Idnurm A, Bahn YSY-S. 2014.
451 *Cryptococcus neoformans* and *Cryptococcus gattii*, the etiologic agents of cryptococcosis.
452 Cold Spring Harb Perspect Med 4:a019760.

453 6. Steele KT, Thakur R, Nthobatsang R, Steenhoff AP, Bisson GP. 2010. In-hospital mortality
454 of HIV-infected cryptococcal meningitis patients with *C. gattii* and *C. neoformans*
455 infection in Gaborone, Botswana. Med Mycol.

456 7. Litvintseva AP, Thakur R, Reller LB, Mitchell TG. 2005. Prevalence of clinical isolates of
457 *Cryptococcus gattii* serotype C among patients with AIDS in Sub-Saharan Africa. J Infect
458 Dis 192:888–892.

459 8. Pappas PG. 2013. Cryptococcal infections in non-HIV-infected patients. Trans Am Clin
460 Climatol Assoc 124:61–79.

461 9. Shih CC, Chen YC, Chang SC, Luh KT, Hsieh WC. 2000. Cryptococcal meningitis in non-HIV-
462 infected patients. QJM 93:245–251.

463 10. Chen S, Sorrell T, Nimmo G, Speed B, Currie B, Ellis D, Marriott D, Pfeiffer T, Parr D, Byth
464 K. 2000. Epidemiology and host- and variety-dependent characteristics of infection due
465 to *Cryptococcus neoformans* in Australia and New Zealand. Australasian Cryptococcal
466 Study Group. Clin Infect Dis 31:499–508.

467 11. Mitchell DH, Sorrell TC, Allworth AM, Heath CH, McGregor AR, Papanaoum K, Richards
468 MJ, Gottlieb T. 1995. Cryptococcal disease of the CNS in immunocompetent hosts:
469 Influence of cryptococcal variety on clinical manifestations and outcome. Clin Infect Dis
470 20:611–616.

471 12. Pappas PG, Perfect JR, Cloud G, Larsen R, Pankey G, Lancaster DJ, Henderson H,
472 Kauffman C, Haas DW, Saccente M, Hamill RJ, Holloway MS, Warren RM, Dismukes WE.
473 2001. Cryptococcosis in human immunodeficiency virus-negative patients in the era of
474 effective azole therapy. Clin Infect Dis 33:690–9.

475 13. Chau TT, Mai NH, Phu NH, Nghia HD, Chuong L V, Sinh DX, Duong V a, Diep PT, Campbell
476 JI, Baker S, Hien TT, Lalloo DG, Farrar JJ, Day JN. 2010. A prospective descriptive study of
477 cryptococcal meningitis in HIV uninfected patients in Vietnam - high prevalence of
478 *Cryptococcus neoformans* var. *grubii* in the absence of underlying disease. BMC Infect Dis
479 10:199.

14. Day JN, Hoang TN, Duong A V, Hong CTT, Diep PT, Campbell JI, Sieu TPM, Hien TT, Bui T, Boni MF, Lalloo DG, Carter D, Baker S, Farrar JJ. 2011. Most cases of cryptococcal meningitis in HIV-uninfected patients in Vietnam are due to a distinct amplified fragment length polymorphism-defined cluster of *Cryptococcus neoformans* var. *grubii* VN1. J Clin Microbiol 49:658–64.

15. Day JN, Qihui S, Thanh LT, Trieu PH, Van AD, Thu NH, Chau TTH, Lan NPHH, Chau NVV, Ashton PM, Thwaites GE, Boni MF, Wolbers M, Nagarajan N, Tan PBOO, Baker S. 2017. Comparative genomics of *Cryptococcus neoformans* var. *grubii* associated with meningitis in HIV infected and uninfected patients in Vietnam. PLoS Negl Trop Dis 11:e0005628.

16. Chen J, Varma A, Diaz M. 2008. *Cryptococcus neoformans* strains and infection in apparently immunocompetent patients, China. Emerg Infect Dis 14.

17. Li Z, Liu Y, Cao H, Huang S, Long M. 2017. Epidemiology and clinical characteristics of cryptococcal meningitis in China (1981-2013): A review of the literature. Med Mycol Open Access 3:1–6.

18. Fan X, Xiao M, Chen S-L, Kong F, Dou H-T, Wang H, Xiao Y-L, Kang M, Sun Z-Y, Hu Z-D, Wan Z, Chen S-L, Liao K, Chu Y-Z, Hu T-S, Zou G-L, Hou X, Zhang L, Zhao Y-P, Xu Y-C, Liu Z-Y. 2016. Predominance of *Cryptococcus neoformans* var. *grubii* multilocus sequence type 5 and emergence of isolates with non-wild-type minimum inhibitory concentrations to fluconazole: a multi-centre study in China. Clin Microbiol Infect 22:887.e1-887.e9.

19. Dou H-T, Xu Y-C, Wang H-Z, Li T-S. 2014. Molecular epidemiology of *Cryptococcus*

neoformans and *Cryptococcus gattii* in China between 2007 and 2013 using multilocus sequence typing and the DiversiLab system. Eur J Clin Microbiol Infect Dis 34:753–62.

20. Choi YH, Ngamskulrungroj P, Varma A, Sionov E, Hwang SM, Carriconde F, Meyer W, Litvintseva AP, Lee WG, Shin JH, Kim E-C, Lee KW, Choi TY, Lee YS, Kwon-Chung KJ. 2010. Prevalence of the VNIc genotype of *Cryptococcus neoformans* in non-HIV-associated cryptococcosis in the Republic of Korea. FEMS Yeast Res 10:769–78.

21. Day JN, Chau TTH, Wolbers M, Mai PP, Dung NT, Mai NH, Phu NH, Nghia HD, Phong ND, Thai CQ, Thai LH, Chuong L V, Sinh DX, Duong V a, Hoang TN, Diep PT, Campbell JI, Sieu TPM, Baker SG, Chau NV V, Hien TT, Lalloo DG, Farrar JJ, Ph D, Chau TTH, Wolbers M, Pham P, Mai PP, Dung NT, Mai NH, Phu NH, Nghia HD, Phong ND, Thai CQ, Thai LH, Chuong L V, Sinh DX, Duong V a, Hoang TN, Diep PT, Campbell JI, Sieu TPM, Baker SG, Chau NV V, Hien TT, Lalloo DG, Farrar JJ. 2013. Combination antifungal therapy for cryptococcal meningitis. N Engl J Med 368:1291–302.

22. Lee A, Toffaletti DL, Tenor J, Soderblom EJ, Thompson JW, Moseley MA, Price M, Perfect JR. 2010. Survival defects of *Cryptococcus neoformans* mutants exposed to human cerebrospinal fluid result in attenuated virulence in an experimental model of meningitis. Infect Immun 78:4213–25.

23. Idnurm A, Walton FJ, Floyd A, Reedy JL, Heitman J. 2009. Identification of ENA1 as a virulence gene of the human pathogenic fungus *Cryptococcus neoformans* through signature-tagged insertional mutagenesis. Eukaryot Cell 8:315–26.

24. Salas SD, Bennett JE, Kwon-Chung KJ, Perfect JR, Williamson PR. 1996. Effect of the

laccase gene CNLAC1, on virulence of *Cryptococcus neoformans*. J Exp Med 184:377–386.

25. Eisenman HC, Mues M, Weber SE, Frases S, Chaskes S, Gerfen G, Casadevall A. 2007. *Cryptococcus neoformans* laccase catalyses melanin synthesis from both D- and L-DOPA. Microbiology 153:3954–3962.

26. Chen SC, Muller M, Zhou JZ, Wright LC, Sorrell TC. 1997. Phospholipase activity in *Cryptococcus neoformans*: a new virulence factor? J Infect Dis 175:414–420.

27. Zaragoza O, Casadevall A. 2004. Experimental modulation of capsule size in *Cryptococcus neoformans*. Biol Proced Online 6:10–15.

28. Hu G, Cheng P-Y, Sham A, Perfect JR, Kronstad JW. 2008. Metabolic adaptation in *Cryptococcus neoformans* during early murine pulmonary infection. Mol Microbiol 69:1456–75.

29. Levitz SM, Tabuni A, Nong SH, Golenbock DT. 1996. Effects of interleukin-10 on human peripheral blood mononuclear cell responses to *Cryptococcus neoformans, Candida albicans*, and lipopolysaccharide. Infect Immun 64:945–51.

30. Fang W, Fa Z, Liao W. 2014. Epidemiology of *Cryptococcus* and cryptococcosis in China. Fungal Genet Biol.

31. Khayhan K, Hagen F, Pan W, Simwami S, Fisher MC, Wahyuningsih R, Chakrabarti A, Chowdhary A, Ikeda R, Taj-Aldeen SJ, Khan Z, Ip M, Imran D, Sjam R, Sriburee P, Liao W, Chaicumpar K, Vuddhakul V, Meyer W, Trilles L, van Iersel LJJ, Meis JF, Klaassen CHW, Boekhout T. 2013. Geographically structured populations of *Cryptococcus neoformans* variety *grubii* in Asia correlate with HIV status and show a clonal population structure.

543 PLoS One 8:e72222.

544 32. Chen M, Xu Y, Hong N, Yang Y, Lei W, Du L, Zhao J, Lei X, Xiong L, Cai L, Xu H, Pan W, Liao
545 W. 2018. Epidemiology of fungal infections in China. Front Med 12:58–75.

546 33. Dou H, Wang H, Xie S, Chen X, Xu Z, Xu Y. 2017. Molecular characterization of
547 *Cryptococcus neoformans* isolated from the environment in Beijing, China. Med Mycol
548 38:1–11.

549 34. Beale MA, Sabiiti W, Robertson EJ, Fuentes-Cabrejo KM, O'Hanlon SJ, Jarvis JN, Loyse A,
550 Meintjes G, Harrison TS, May RC, Fisher MC, Bicanic T. 2015. Genotypic diversity is
551 associated with clinical outcome and phenotype in cryptococcal meningitis across
552 Southern Africa. PLoS Negl Trop Dis 9:e0003847.

553 35. Bojarczuk A, Miller KA, Hotham R, Lewis A, Ogryzko N V., Kamuyango AA, Frost H, Gibson
554 RH, Stillman E, May RC, Renshaw SA, Johnston SA. 2016. *Cryptococcus neoformans*
555 intracellular proliferation and capsule size determines early macrophage control of
556 Infection. Sci Rep 6:21489.

557 36. Zaragoza O, Chrisman CJ, Castelli MV, Frases S, Cuenca-Estrella M, Rodríguez-Tudela JL,
558 Casadevall A. 2008. Capsule enlargement in *Cryptococcus neoformans* confers resistance
559 to oxidative stress suggesting a mechanism for intracellular survival. Cell Microbiol
560 10:2043–2057.

561 37. García-Rodas R, Casadevall A, Rodríguez-Tudela JL, Cuenca-Estrella M, Zaragoza O. 2011.
562 *Cryptococcus neoformans* capsular enlargement and cellular gigantism during *Galleria*
563 *mellonella* infection. PLoS One 6:e24485.

564 38. Robertson EJ, Najjuka G, Rolfes M a, Akampurira A, Jain N, Anantharanjit J, von
565 Hohenberg M, Tassieri M, Carlsson A, Meya DB, Harrison TS, Fries BC, Boulware DR,
566 Bicanic T. 2014. *Cryptococcus neoformans ex vivo* capsule size is associated with
567 intracranial pressure and host immune response in HIV-associated cryptococcal
568 meningitis. J Infect Dis 209:74–82.

569 39. Vecchiarelli A, Pericolini E, Gabrielli E, Chow S-K, Bistoni F, Cenci E, Casadevall A. 2011.
570 *Cryptococcus neoformans* galactoxylomannan is a potent negative immunomodulator,
571 inspiring new approaches in anti-inflammatory immunotherapy. Immunotherapy 3:997–
572 1005.

573 40. Kronstad J, Saikia S, Nielson ED, Kretschmer M, Jung W, Hu G, Geddes JMH, Griffiths EJ,
574 Choi J, Cadieux B, Caza M, Attarian R. 2012. Adaptation of *Cryptococcus neoformans* to
575 mammalian hosts: integrated regulation of metabolism and virulence. Eukaryot Cell
576 11:109–18.

577 41. Botts MR, Giles SS, Gates MA, Kozel TR, Hull CM. 2009. Isolation and characterization of
578 *Cryptococcus neoformans* spores reveal a critical role for capsule biosynthesis genes in
579 spore biogenesis. Eukaryot Cell 8:595–605.

580 42. Bódi Z, Farkas Z, Nevozhay D, Kalapis D, Lázár V, Csörgő B, Nyerges Á, Szamecz B, Fekete
581 G, Papp B, Araújo H, Oliveira JL, Moura G, Santos MASS, Székely T, Balázsi G, Pál C. 2017.
582 Phenotypic heterogeneity promotes adaptive evolution. PLoS Biol 15:e2000644.

583 43. Chow EWL, Morrow CA, Djordjevic JT, Wood IA, Fraser JA. 2012. Microevolution of
584 *Cryptococcus neoformans* driven by massive tandem gene amplification. Mol Biol Evol

29:1987–2000.

44. Zaragoza O, Alvarez M, Telzak A, Rivera J, Casadevall A. 2007. The relative susceptibility of mouse strains to pulmonary *Cryptococcus neoformans* infection is associated with pleiotropic differences in the immune response. Infect Immun 75:2729–39.

45. Cheng P-Y, Sham A, Kronstad JW. 2009. *Cryptococcus gattii* isolates from the British Columbia cryptococcosis outbreak induce less protective inflammation in a murine model of infection than *Cryptococcus neoformans*. Infect Immun 77:4284–94.

46. Sellers RS, Clifford CB, Treuting PM, Brayton C. 2012. Immunological variation between inbred laboratory mouse strains: Points to consider in phenotyping genetically immunomodified mice. Vet Pathol 49:32–43.

47. Lortholary O, Improvisi L, Rayhane N, Gray F, Fitting C, Cavaillon JM, Dromer F. 1999. Cytokine profiles of AIDS patients are similar to those of mice with disseminated *Cryptococcus neoformans* infection. Infect Immun 67:6314–20.

48. Jain A V, Zhang Y, Fields WB, McNamara D a, Choe MY, Chen G-H, Erb-Downward J, Osterholzer JJ, Toews GB, Huffnagle GB, Olszewski M a. 2009. Th2 but not Th1 immune bias results in altered lung functions in a murine model of pulmonary *Cryptococcus neoformans* infection. Infect Immun 77:5389–99.

49. Koguchi Y, Kawakami K. 2002. Cryptococcal infection and Th1-Th2 cytokine balance. Int Rev Immunol 21:423–38.

50. Chaka W, Verheul AF, Vaishnav V V, Cherniak R, Scharringa J, Verhoef J, Snippe H, Hoepelman IM. 1997. *Cryptococcus neoformans* and cryptococcal glucuronoxylomannan,

galactoxylomannan, and mannoprotein induce different levels of tumor necrosis factor alpha in human peripheral blood mononuclear cells. Infect Immun 65:272–8.

51. Levitz SM, Tabuni A, Kornfeld H, Reardon CC, Golenbock DT. 1994. Production of tumor necrosis factor alpha in human leukocytes stimulated by *Cryptococcus neoformans*. Infect Immun 62:1975–81.

52. García-Rivera J, Casadevall A. 2001. Melanization of *Cryptococcus neoformans* reduces its susceptibility to the antimicrobial effects of silver nitrate. Med Mycol 39:353–357.

FIGURE LEGENDS

Figure 1. *In vitro* induced capsule thickness and cell diameter of individual *Cryptococcus neoformans* strains from Vietnam: Cells were grown on DMEM medium/5% CO_2 and visually assessed by India ink staining. Images were taken for single cells measurement using ImageJ software. Capsule thickness is obtained by subtracting cell body diameter from total cell diameter. AFLP-VNI-γ/MLST-ST5 strains expressed higher degree of variation in both capsule size and cell diameter *in vitro*, which remains significant even when the outlier BMD1646 was removed from the analysis (p<0.0001 for both capsule and cell size, Fligner-Killeen test). Scattered plot represents single cells from an individual strain. Data for individual strains are presented as mean with error bars denoting standard deviation. Strains selected for experiment in mice were indicated by asterisks.

626 **Figure 2. Kaplan-Meier survival curves for mice infected with either ST5 (n = 5) or non-ST5 (n=**
627 **3) *Cryptococcus neoformans* strains**. 10 mice were infected per strain (n = 80). Mice were
628 monitored daily until the point of more than 15% weight loss or visible suffering and were then
629 sacrificed by CO_2 inhalation. Mice infected with ST5 strains had statistically significantly longer
630 survival times than those infected with non-ST5 strains (P<0.0001, Mantel-Cox log rank test).

631

632 **Figure 3. Fungal burden in lung and brain tissue at days 7, 14 and the point of impending**
633 **death (mortality experiment) according to infecting genotype.** For day 7 and day 14, five mice
634 were infected with each isolate (5 ST5 isolates and 3 ST4 isolates, N=80 in total). Mice were
635 monitored daily. No mice needed to be sacrificed prior to Day 14 for distress. The fungal burden
636 in non-ST5 infections was higher than in ST5 infections in both lung tissue at all time points, and
637 in brain tissue at the point of sacrifice. For P values see text. Boxplots (Tukey's method)
638 describe the median and interquartile range, the whiskers demarcate the largest or smallest
639 values that were not outliers (black dots); outliers are defined as more than 1.5 times the
640 interquartile range from the nearest quartile.

641

642 **Figure 4. Genotype-specific cytokine concentrations from lung homogenate of A/J mice at 7**
643 **and 14 days post infection with $5x10^4$ *C. neoformans* cells/mouse.** Five mice were infected
644 with each strain from each genotype at each time points. ST5 strains induced significantly
645 higher levels of TNF-α at day 7, suggesting an earlier and more profound initial inflammatory
646 response in infected mice. By day 14 mice infected with non-ST5 strains have higher levels

proinflammatory cytokines, probably a result of ST5 yeasts being cleared more rapidly from infected mice. The horizontal line within the box indicates the median; boundaries of the box indicate the 25^{th} and 75^{th} percentile and the whiskers indicate the highest and lowest values of the results; outliers are denoted as black dots (Tukey's method). Data are standardized as picograms of cytokine per gram lung tissue. Asterisks indicate statistically significant differences (Mann-Whitney test).

Figure 5. Genotype-specific changes in cytokine concentrations from lung homogenate of A/J mice infected with *C. neoformans* between day 7 and day 14 post-infection. Box and whisker plots (Tukey's method) compare levels of each cytokine between day 7 and day 14 for each genotype. Data are standardized as picograms of cytokine per gram lung tissue. Asterisks indicate statistically significant differences (Mann-Whitney test).

Figure 6. Periodic Acid Schiff (PAS) staining of pulmonary tissue from mice infected with BMD1338 and BMD1415 on days 7 and 14. The two strains represent ST5 and non-ST5, respectively. A/J mice were inoculated intranasally with $5x10^4$ yeast cells. Lung specimens were harvested at days 7 and 14 for histopathological examination. Photomicrographs were obtained at 200X magnification; the scale bar represents 215 µm). (A-B): lung sections from mice infected with BMD1338 (VNI-γ/ST5) at day 7 and day 14, respectively. (C-D): lung sections from mice infected with BMD1415 (VNI-δ/ST4) at day 7 and day 14, respectively. Perivascular infiltration (red arrows) and necrosis are more marked by day 14 for both strains. Encapsulated yeasts

(yellow arrows), notable for the larger cell size and capsule thickness of BMD 1338 compared with BMD1415.

Figure 7. Mucicarmine staining of capsular material in paraffin-embedded mice pulmonary tissue.

Uninflated lung specimens were harvested from mice as described in the methods. Mucicarmine staining was performed to visualize the cryptococcal capsule. Photomicrographs were captured at 400X magnification with scale bar indicating 55µm. Capsular polysaccharide is stained pink (indicated by blue arrows), demonstrating diffuse localization consistent with extensive capsule production by yeasts in the alveolar space.

690

691

692

693

694 **TABLES**

695 **TABLE 1** *Cryptococcus neoformans* isolate clinical source and typing (n=30).

Isolate data				Patient data	
Order	Strain name	AFLP cluster	MLST	Underlying Disease	Sex
1	BK14	VNI-δ	4	HIV	M
2	BK163	VNI-δ	4	HIV	M
4	BK225	VNI-δ	4	HIV	M
6	BK48	VNI-δ	4	HIV	M
7	BK59	VNI-δ	4	HIV	F
8	BK69	VNI-δ	4	HIV	M
9	BK74	VNI-δ	4	HIV	M
10	BK80*	VNI-δ	4	HIV	M
11	BK87	VNI-δ	4	HIV	M
12	BK88	VNI-δ	4	HIV	M
13	BK89	VNI-δ	4	HIV	M
15	BMD1415*	VNI-δ	4	Lupus	M
3	BK218	VNI-δ	6	HIV	M
5	BK234	VNI-δ	6	HIV	F
14	BMD1367*	VNI-δ	306	Gastric cancer	F
16	BK147*	VNI- γ	5	HIV	M
17	BK44*	VNI-γ	5	HIV	M
18	BMD101	VNI-γ	5	None known	M
19	BMD1228	VNI-γ	5	None known	F
20	BMD1291	VNI-γ	5	None known	F
21	BMD1338*	VNI-γ	5	None known	M
22	BMD1353	VNI-γ	5	None known	M
23	BMD1452	VNI-γ	5	None known	F
24	BMD1646*	VNI-γ	5	None known	M
25	BMD1716	VNI-γ	5	None known	F
26	BMD367	VNI-γ	5	None known	M
27	BMD673	VNI-γ	5	None known	F

28	BMD700*	VNI-γ	5	None known	M
29	BMD854	VNI-γ	5	None known	F
30	BMD899	VNI-γ	5	None known	F

AFLP = amplified fragment length polymorphism

MLST = multi locus sequence typing

M = Male, F = Female

** indicates isolates selected for mouse experiment*

TABLE 2 Variability in *in vitro* capsule thickness and cell diameter of *Cryptococcus neoformans* strains by Sequence Type (ST)

	MLST Group	
Variable	**ST5**	**Non-ST5**
Capsule Thickness (µm)		
Mean*	2.64	2.01
95% CI	2.49 - 2.79	1.94 - 2.07
Range	0.01 - 9.56	0.02 - 6.16
Coefficient of Variation[$] (%)	0.63	0.37
Cell diameter (µm)		
Mean*	11.38	9.69
95% CI of Mean	10.96 - 11.79	9.52 - 9.87
Range	4.74 - 27.22	5.25 - 19.89
Coefficient of Variation[$] (%)	0.41	0.20

** P<0.0001, t-test with Welch's correction.*

[$] *P< 0.0001, Fligner-Killeen test of homogeneity of variance.*

711 **TABLE 3** Tissue fungal burden in lung and brains of mice at days 7, 14 and at time of death by infecting

712 MLST Sequence Type (ST)

	Fungal burden (Mean log_{10} colony forming units per gram of tissue) [95%CI]		
Tissue	**ST5**	**Non-ST5**	**P Value**
Lung (Day 7)	4.96 [3.86 - 6.05]	7.07 [6.85 - 7.29]*	<0.001
Brain (Day 7)	0.81 [0.38 - 1.24]	1.59 [0.87 - 2.30]	0.054
Lung (Day 14)	5.48 [4.34 - 6.62]	8.00 [7.77 - 8.23]*	<0.0001
Brain (Day 14)	1.56 [0.81 - 2.31]	1.91 [1.12 - 2.69]	0.36
Lung (Death)	3.81 [3.05 - 4.57]	6.53 [6.30 - 6.76]*	<0.0001
Brain (Death)	2.90 [2.23 - 3.56]	4.29 [3.90 - 4.68]*	0.01

**Mann-Whitney test.*

713

714

715

716

717

718

719

720 **TABLE 4:** Cytokine concentrations from lung homogenate of infected mice at day 7 and day 14 post-

721 infection according to infecting *Cryptococcus neoformans* Sequence Type (ST)

		Mean cytokine concentration (pg per gram of lung tissue) [95%CI]		
Cytokine		**ST5**	**Non-ST5**	***P Value (ST5 vs non-ST5)**
Day 7				
Th-1	IL-12	853.12 [750.50 - 955.80]	822.87 [608.90 - 1037.00]	0.30
	IFN-γ	136.02 [115.00 - 157.00]	150.59 [105.80 - 195.30]	0.97
	TNF-α	3933.71 [3486.00 - 4381.00]	3256.25 [2630.00 – 3882.00]	**0.01**
Th-2	IL-4	230.79 [162.80 - 298.80]	253.24 [11.60 - 349.90]	0.92
	IL-5	561.05 [369.00 - 753.10]	459.85 [344.40 - 575.40]	0.91
	IL-10	145.01 [128.20 - 161.80]	139.99 [119.30 - 160.70]	0.68
Th-17	IL-17	268.48 [155.90 – 381.00]	243.41 [165.60 - 321.20]	0.24
TNF-α/IL-10 ratio		27.13	23.26	ND
Day 14				
Th-1	IL-12	547.84 [412.40 - 683.30]	213.72 [120.50 - 306.90]	**<0.01**
	IFN-γ	91.2 [57.25 - 125.20]	1760.67 [166.50 - 3355.00]	0.09
	TNF-α	2802.36 [2385.00 - 3220.00]	6378.76 [3374.00 - 9384.00]	**<0.01**
Th-2	IL-4	1154.72 [673.50 – 636.00]	800.35 [604.70 – 996.00]	0.60
	IL-5	294.6 [170.40 - 418.80]	347.55 [279.20 - 415.90]	0.15
	IL-10	132.76 [102.10 - 163.40]	220.15 [172.40 - 267.90]	**0.01**
Th-17	IL-17	175.75 [65.54 – 286.00]	1012.49 [459.20 – 1566.00]	**0.01**
TNF-α/IL-10 ratio		21.11	28.97	ND

722 ** Mann-Whitney test. ND: not done*

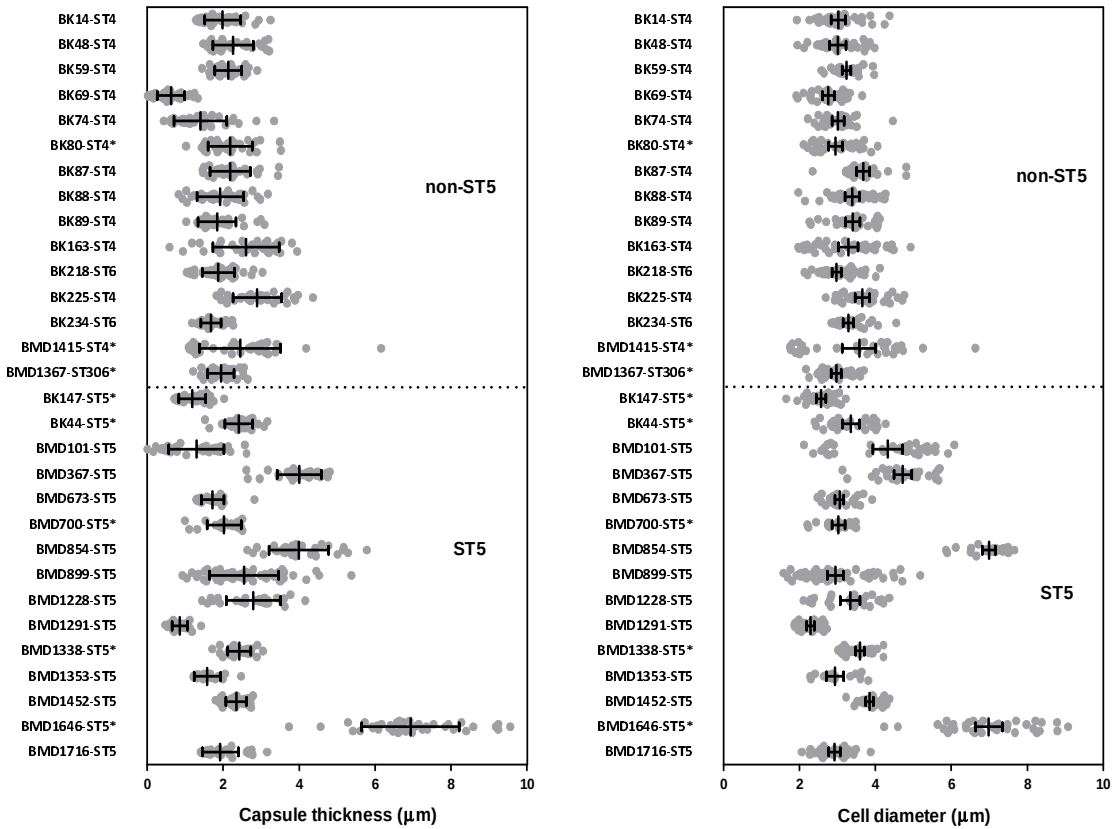

Figure 1. *In vitro* induced capsule thickness and cell diameter of individual *Cryptococcus neoformans* strains from Vietnam: Cells were grown on DMEM medium/5% CO_2 and visually assessed by India ink staining. Images were taken for single cells measurement using ImageJ software. Capsule thickness is obtained by subtracting cell body diameter from total cell diameter. AFLP-VNI-γ/MLST-ST5 strains expressed higher degree of variation in both capsule size and cell diameter *in vitro*, which remains significant even when the outlier BMD1646 was removed from the

analysis (p<0.0001 for both capsule and cell size, Fligner-Killeen test). Scattered plot represents single cells from an individual strain. Data for individual strains are presented as mean with error bars denoting standard deviation. Strains selected for experiment in mice were indicated by asterisks.

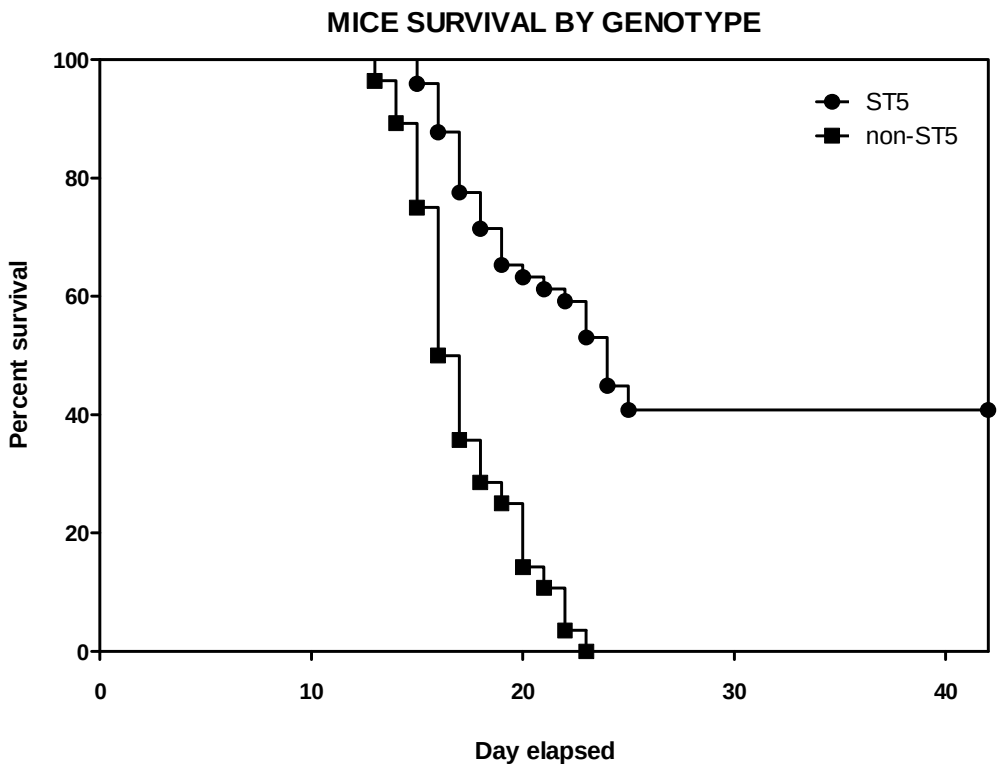

Figure 2. Kaplan-Meier survival curves for mice infected with either ST5 (n = 5) or non-ST5 (n= 3) *Cryptococcus neoformans* strains. 10 mice were infected per strain (n = 80). Mice were monitored daily until the point of more than 15% weight loss or visible suffering and were then sacrificed by CO_2 inhalation. Mice infected with ST5 strains had statistically significantly longer survival times than those infected with non-ST5 strains (P<0.0001, Mantel-Cox log rank test).

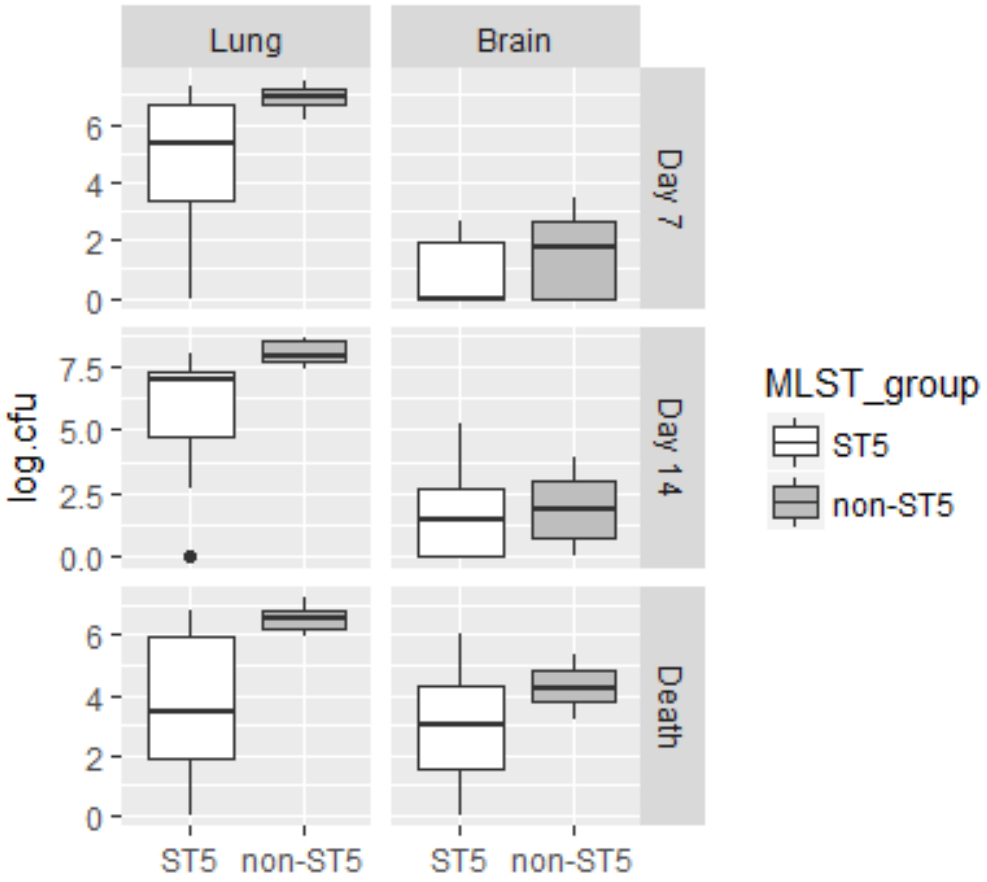

Figure 3. Fungal burden in lung and brain tissue at days 7, 14 and the point of impending death (mortality experiment) according to infecting genotype. For day 7 and day 14, five mice were infected with each isolate (5 ST5 isolates and 3 ST4 isolates, N=80 in total). Mice were monitored daily. No mice needed to be sacrificed prior to Day 14 for distress. The fungal burden in non-ST5 infections was higher than in ST5

infections in both lung tissue at all time points, and in brain tissue at the point of sacrifice. For P values see text. Boxplots (Tukey's method) describe the median and interquartile range, the whiskers demarcate the largest or smallest values that were not outliers (black dots); outliers are defined as more than 1.5 times the interquartile range from the nearest quartile.

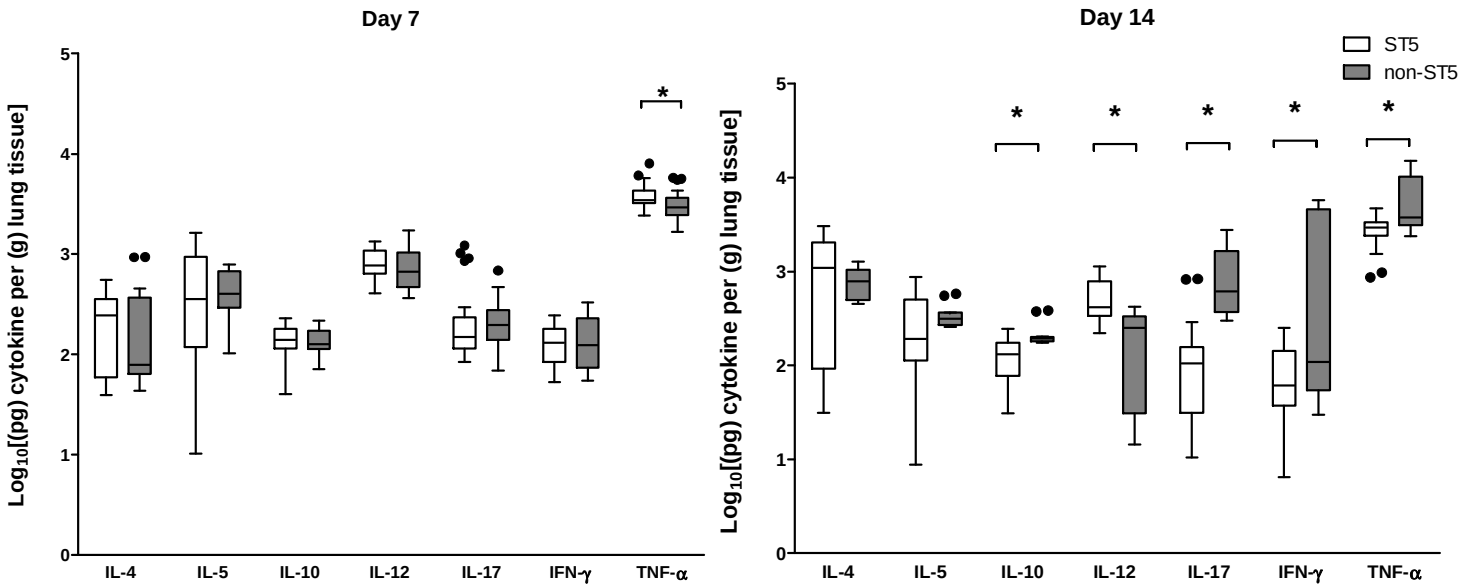

Figure 4. Genotype-specific cytokine concentrations from lung homogenate of A/J mice at 7 and 14 days post infection with 5x10^4 *C. neoformans* cells/mouse. Five mice were infected with each strain from each genotype at each time points. ST5 strains induced significantly higher levels of TNF-α at day 7, suggesting an earlier and more profound initial inflammatory response in infected mice. By day 14 mice infected with non-ST5 strains have higher levels proinflammatory cytokines, probably a result of ST5 yeasts being cleared more rapidly from infected mice. The horizontal line within the box indicates the median; boundaries of the box indicate the 25th and 75th percentile and the whiskers

indicate the highest and lowest values of the results; outliers are denoted as black dots (Tukey's method). Data are standardized as picograms of cytokine per gram lung tissue. Asterisks indicate statistically significant differences (Mann-Whitney test).

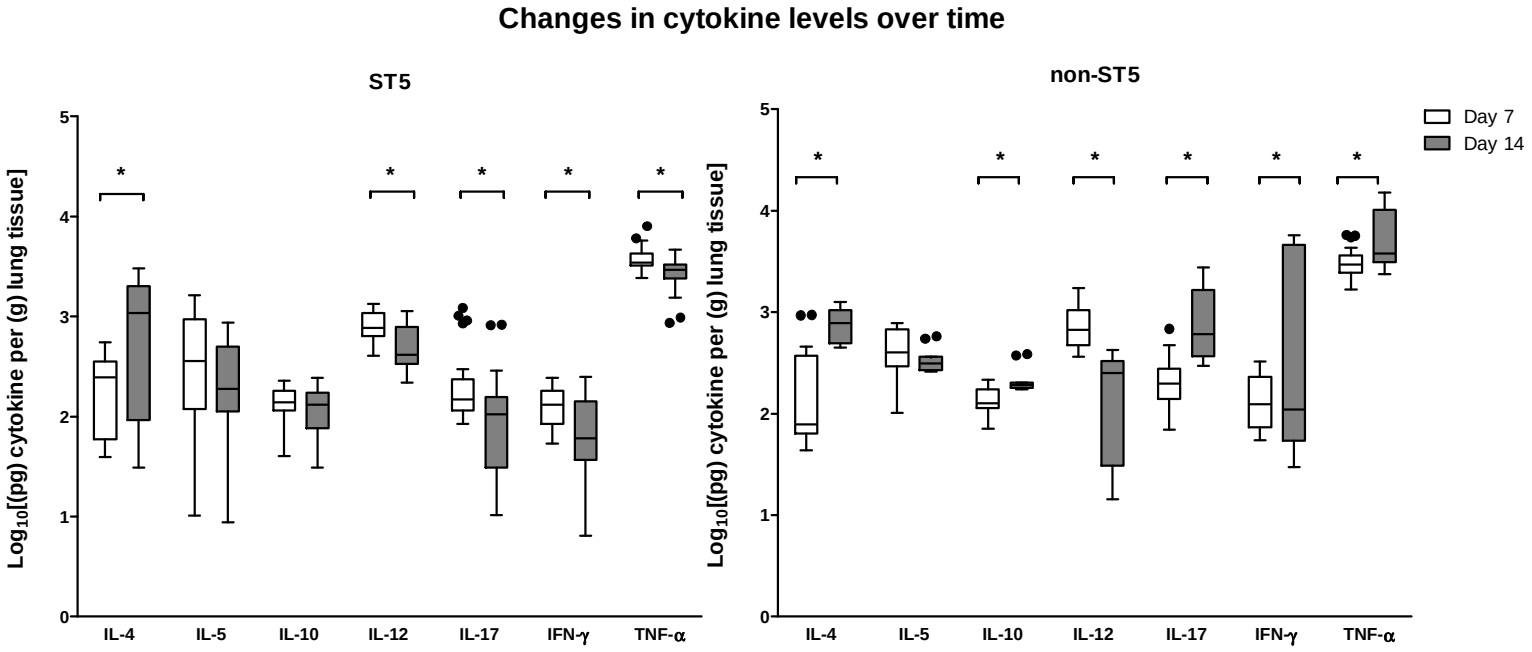

Figure 5. Genotype-specific changes in cytokine concentrations from lung homogenate of A/J mice infected with *C. neoformans* between day 7 and day 14 post-infection. Box and whisker plots (Tukey's method) compare levels of each cytokine between day 7 and day 14 for each genotype. Data are standardized as picograms of cytokine per gram lung tissue. Asterisks indicate statistically significant differences (Mann-Whitney test).

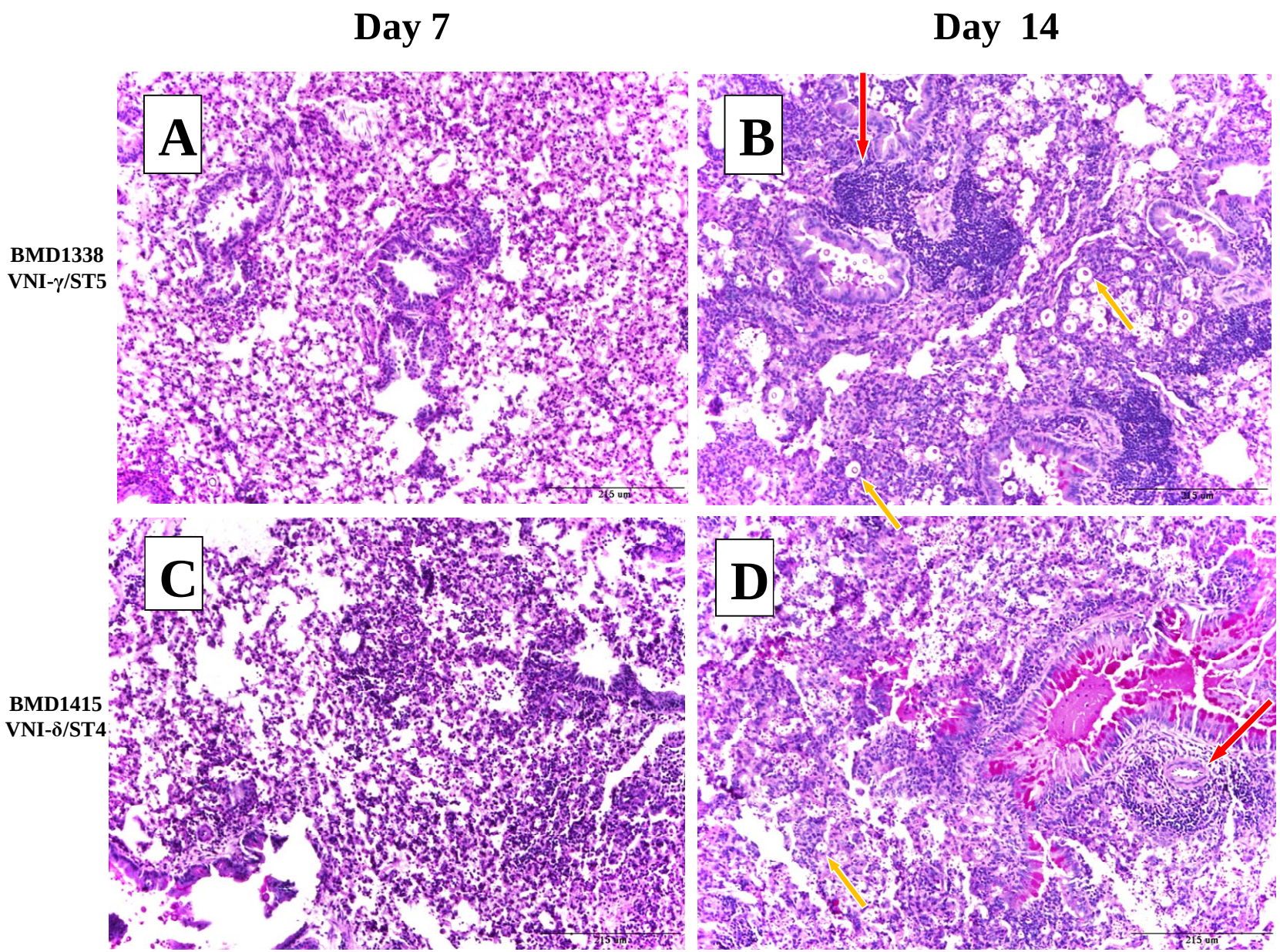

Figure 6. Periodic Acid Schiff (PAS) staining of pulmonary tissue from mice infected with BMD1338 and BMD1415 on days 7 and 14. The two strains represent ST5 and non-ST5, respectively. A/J mice were inoculated intranasally with $5x10^4$ yeast cells. Lung specimens were harvested at days 7 and 14 for histopathological examination. Photomicrographs were obtained at 200X magnification; the scale bar represents 215 µm). (A-B): lung sections from mice infected with BMD1338 (VNI-γ/ST5) at day 7 and day 14, respectively. (C-D): lung sections from mice infected with BMD1415 (VNI-δ/ST4) at day 7 and day 14, respectively. Perivascular infiltration (red arrows) and necrosis are more marked by day 14 for both strains. Encapsulated yeasts (yellow arrows), notable for the larger cell size and capsule thickness of BMD 1338 compared with BMD1415.

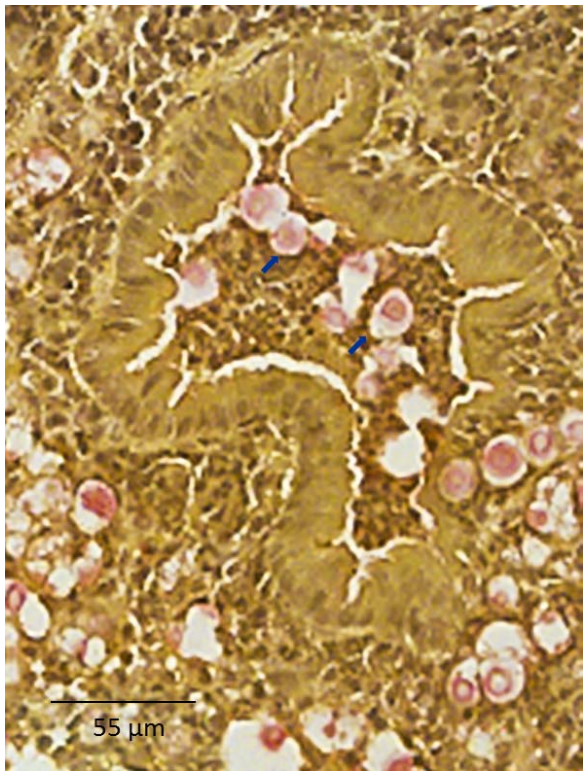

Figure 7. Mucicarmine staining of capsular material in paraffin-embedded mice pulmonary tissue.

Uninflated lung specimens were harvested from mice as described in the methods. Mucicarmine staining was performed to visualize the cryptococcal capsule. Photomicrographs were captured at 400X magnification with scale bar indicating 55µm. Capsular polysaccharide is stained pink (indicated by blue arrows), demonstrating diffuse localization consistent with extensive capsule production by yeasts in the alveolar space.